nature chemical biology

Article

https://doi.org/10.1038/s41589-023-01463-7

Protein-based bandpass filters for controlling cellular signaling with chemical inputs

Received: 10 February 2023

Accepted: 29 September 2023

Published online: 13 November 2023

Check for updates

Sailan Shui[1,2], Leo Scheller[1,2] & Bruno E. Correia[1,2]

Biological signal processing is vital for cellular function. Similar to electronic circuits, cells process signals via integrated mechanisms. In electronics, bandpass filters transmit frequencies with defined ranges, but protein-based counterparts for controlled responses are lacking in engineered biological systems. Here, we rationally design protein-based, chemically responsive bandpass filters (CBPs) showing OFF-ON-OFF patterns that respond to chemical concentrations within a specific range and reject concentrations outside that range. Employing structure-based strategies, we designed a heterodimeric construct that dimerizes in response to low concentrations of a small molecule (ON), and dissociates at high concentrations of the same molecule (OFF). The CBPs have a multidomain architecture in which we used known drug receptors, a computationally designed protein binder and small-molecule inhibitors. This modular system allows fine-tuning for optimal performance in terms of bandwidth, response, cutoff and fold changes. The CBPs were used to regulate cell surface receptor signaling pathways to control cellular activities in engineered cells.

Cells are sophisticated signal-processing units that respond and adapt to environmental and internal signals[1]. Synthetic biologists strive to engineer cells that process signals in a systematic, predictable, controllable and integrated manner[2]. Chemically responsive protein modules are particularly useful for engineering artificial cellular activities controlled by external cues[1,3]. Currently available protein switches sense a specific chemical and control the activity of biological circuits through induced protein–protein association (for example, rapamycin-induced FKBP–FRB dimerization[4]) or dissociation (chemically disruptable heterodimers[5]). Protein switches are capable of up- or downregulation of cellular activities, but require a high dilution of the chemicals to revert the controlled cellular activity from ON to OFF, or vice versa[3]. However, cells perceive and respond to temporal and spatial stimulations in a timely and efficient manner[6]. For instance, processes that result in pattern formation are a hallmark of such coordinated and complex behavior. Current engineered protein components mostly up- or downregulate outputs in a uniform manner, and therefore engineered cellular systems often fail in replicating such sophisticated signal-processing events.

Morphogen-driven pattern organization is a hallmark of coordination of cell behavior and signal detection of gradient concentrations. To engineer morphogen function, many efforts have been focused on developing band-detecting systems that mimic electronic bandpass filters[7]. An electronic bandpass filter can pass frequencies within a defined range, and reject frequencies outside that range. Bandpass filters have been engineered in biological systems by tuning the affinity of a trans-repressor for the acyl-homoserine lactone signaling molecule and dosing with different plasmid copies[8]. Bandpass filters were also designed through a dual approach of positive and negative genetic selections for β-lactamase activity. Cellular β-lactamase activity was directed by an IPTG-inducible promoter, regulating cell growth exclusively within a defined range in the presence of the β-lactam antibiotics ampicillin and tetracycline[9]. The cellular β-lactamase activity-detecting bandpass filter was used to demonstrate the effects

[1]Laboratory of Protein Design and Immunoengineering (LPDI)-STI-EPFL, Lausanne, Switzerland. [2]Swiss Institute of Bioinformatics (SIB), Lausanne, Switzerland. e-mail: bruno.correia@epfl.ch

https://doi.org/10.1038/s41589-023-01463-7

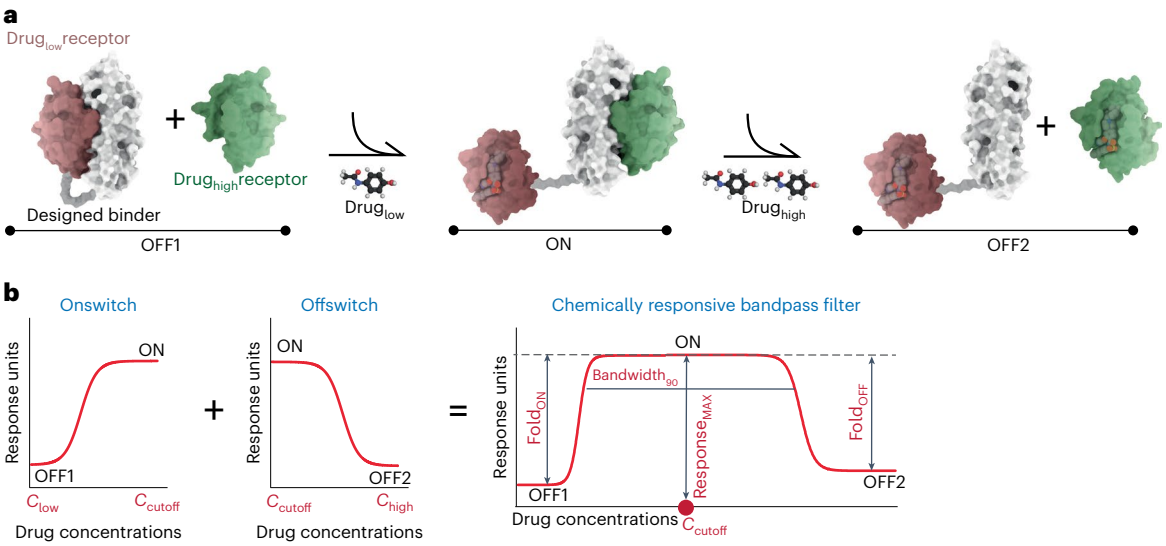

Fig. 1 | Design strategy and performance parameters of the chemically responsive protein-based bandpass filters. a, Schematic representation of the CBP mode of action. Each CBP contains three proteins: the designed binder (white surface representation) and two drug receptors (drug$_{low}$ receptor in red and drug$_{high}$ receptor in green). For low drug concentrations, CBPs switch to the ON state, and in high drug concentrations CBPs switch to the OFF2 state. **b**, Design principles of the CBPs by integrating an ON switch (from low drug concentration to cutoff drug concentration) and an OFF switch (from cutoff drug concentration to high drug concentration), and the tunable parameters of each CBP, including cutoff concentration (C_{cutoff}, drug concentration of Response$_{MAX}$), bandwidth (Bandwidth$_{90}$, drug concentration range maintains ≥90% of Response$_{MAX}$), fold changes (Fold$_{ON}$ = Response$_{MAX}$/Response$_{OFF1}$, Fold$_{OFF}$ = Response$_{MAX}$/Response$_{OFF2}$) and the maximum response (Response$_{MAX}$).

of multiple morphogen gradients on cell survival[10]; furthermore, this bandpass filter has been adapted to select protein–protein interactions of different binding strength[11]. Artificial bacterial transcription factors have also been designed to sense and respond to D-fucose and IPTG to mimic band-detecting behavior[12]. Other biological networks with band-detecting characteristics have been developed on the basis of transcription factors, including detection of L-arabinose[13] and nisin[14]. Similar work has also been done in mammalian systems, where a synthetic genetic network was constructed with bandpass characteristics in which output expression is only 'ON' across a window of low concentrations of tetracycline[15].

Despite these examples of genetic bandpass circuitry, there are no engineered protein-based sensors that do not rely on transcriptional regulation systems that can perform such behaviors. There are also limitations in terms of the choice of transcription factors and small-molecule inducers that can be used in genetic circuits. To overcome these limitations, a generalizable approach for engineering robust protein-based bandpass filters is needed. Hence, we rationally designed CBPs that detect drug concentrations, pass concentrations within a certain range and reject concentrations beyond that range, resulting in an 'OFF-ON-OFF' regulatory pattern. Each CBP consists of three distinct protein components: a designed binder and a drug$_{low}$ receptor and a drug$_{high}$ receptor that are sensitive to drug disruption in low and high concentrations, respectively. Each CBP undergoes an 'ON switch' process, where the designed binder dissociates from the drug$_{low}$ receptor at low drug concentrations and consequently binds to the drug$_{high}$ receptor, and an 'OFF switch' process, where the designed binder dissociates from the drug$_{high}$ receptor at high drug concentrations (Fig. 1a). On the basis of the unique behavior of the CBPs, we identified five key parameters, including fold changes between the ON state and two OFF states, maximum response, cutoff concentration and bandwidth, which can be tuned to sustain the activity controlled by CBP at a defined level (Fig. 1b). These protein-based CBPs are highly modular; the binding affinities between the drug receptors and the designed binder, as well as the drug sensitivities of the drug receptors, can be modulated to adjust the parameters of the CBPs. Furthermore, the designed CBPs were incorporated in cell surface receptors to regulate signaling pathways externally in a bandpass filtering fashion. Our results show the potential of rationally designed protein-based CBPs for diverse cellular applications.

Results

Bandpass filter design by integrating ON and OFF switches

Analogous to electronic bandpass filters, we sought to design CBPs with an OFF-ON-OFF regulatory pattern depending on the concentration of a drug. To do so, three proteins were used to construct a CBP: a designed binder that interacts with both drug receptors, a drug receptor that is dissociated from the designed binder at low drug concentrations (drug$_{low}$ receptor) and a drug receptor that can only be dissociated at high drug concentrations (drug$_{high}$ receptor). The designed binder is fused to the drug$_{low}$ receptor via a $(GGGGS)_3$ linker (OFF1 state, intramolecular dimerization, intermolecular dissociation), is dissociated from the drug$_{low}$ receptor to bind to the drug$_{high}$ receptor at low drug concentrations (ON state, intermolecular dimerization) and is dissociated from both drug receptors at high drug concentrations (OFF2 state) (Fig. 1a).

Biological activities controlled by CBPs are designed to be upregulated and then downregulated with increasing drug concentrations. We hypothesized that the up- and downregulation could be mimicked by integrating a protein-based ON switch, which turns biological activity ON from low to cutoff concentrations (from OFF1 state to ON state), and an OFF switch, which turns biological activity OFF from cutoff to high concentrations (from ON state to OFF2 state) (Fig. 1b, left). Many parameters of CBPs can be characterized and modulated. Beyond fold changes and maximum response, we also monitored the cutoff concentration indicating the highest response that can be achieved, and the bandwidth indicating the range of drug concentrations that retain the ON state (Fig. 1b, right).

Dual-drug-responsive cell surface receptors

Bcl2 and its homologous protein, BclXL, are primarily responsible for exerting anti-apoptotic functions by binding to the BH3 domain of

https://doi.org/10.1038/s41589-023-01463-7

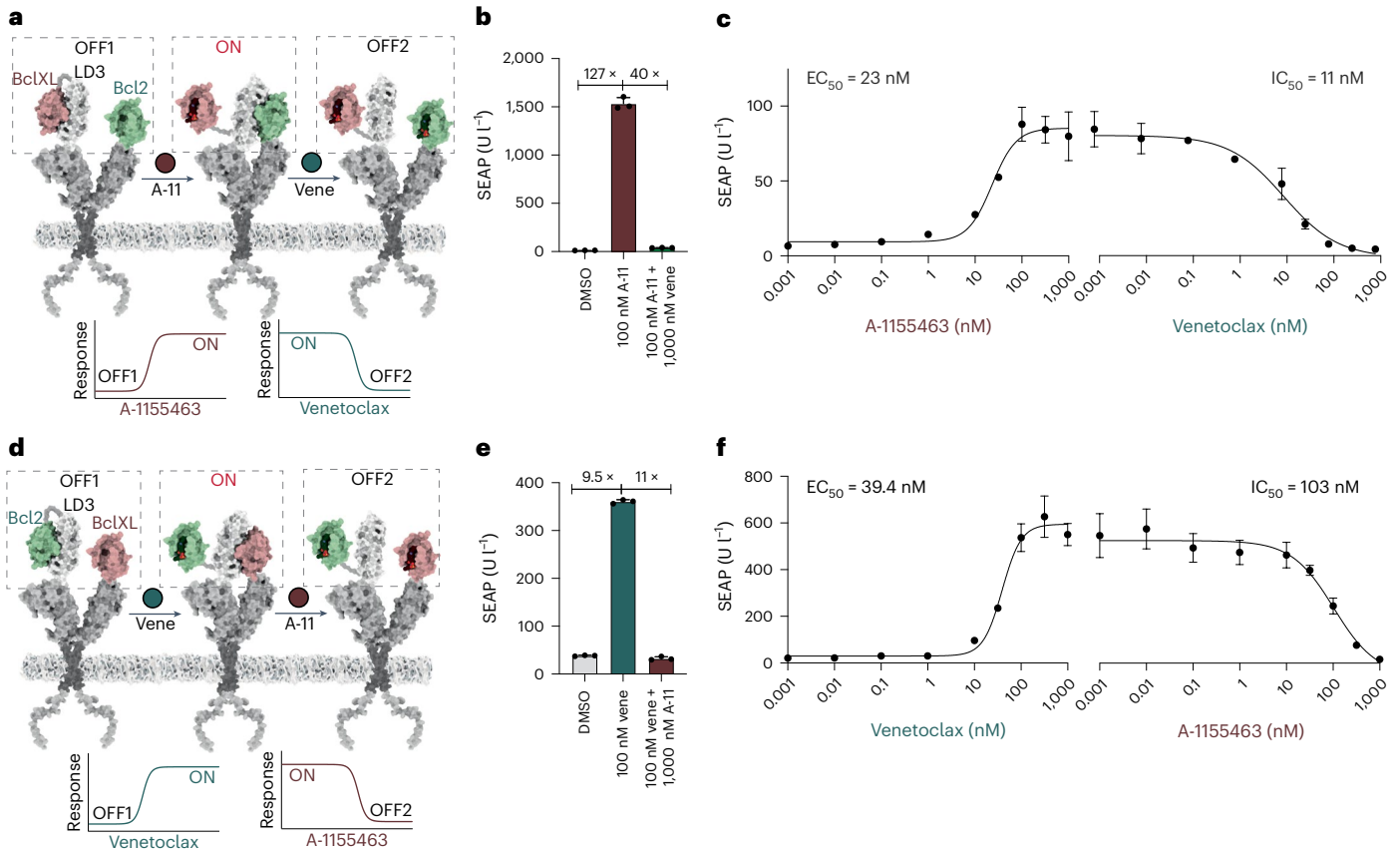

Fig. 2 | Dual-drug-controlled switches based on BclXL and Bcl2 proteins controlled by two sequential chemical inputs mimicking the CBP behavior. **a**, Scheme of Bcl2 and BclXL–LD3 complex fused to GEMS. The GEMS with the dual-drug-controlled (A-1155463, venetoclax) switch is initially in the OFF1 state and can be switched to the ON state by the BclXL inhibitor A-1155463 (A-11; red circle), and can be switched to the OFF2 state by the Bcl2 inhibitor venetoclax (vene; green circle). The curves on the bottom show the idealized output target for switching between states. **b**, Fold change of GEMS with the dual-drug-controlled (A-1155463, venetoclax) switch between no drug treatment (DMSO) versus 100 nM A-1155463 (ON) versus 100 nM A-1155463 and 1 μM venetoclax (OFF), showing SEAP expression after 24 h. Each bar represents the mean of three biological replicates ± s.d., overlaid with the original data points. **c**, Dose responses in engineered cells expressing GEMS with the dual-drug-controlled (A-1155463, venetoclax) switch. Each data point represents the mean ± s.d. of three replicates. The EC_{50} values of the ON phase and IC_{50} values of the OFF phase were calculated individually using four-parameter nonlinear regression. **d**, Scheme of BclXL and Bcl2–LD3 complex fused to GEMS. The GEMS with the dual-drug-controlled (venetoclax, A-1155463) switch can be turned to the ON state by the Bcl2 inhibitor venetoclax (vene; green circle) and OFF with the BclXL inhibitor A-1155463 (A-11; red circle). The curves on the bottom show the idealized output target for switching between states. **e**, Fold change of GEMS with the dual-drug-controlled (venetoclax, A-1155463) switch activity between no drug treatment (DMSO) versus 100 nM venetoclax (ON) versus 100 nM venetoclax and 1 μM A-1155463 (OFF), showing SEAP expression after 24 h. Each bar represents the mean of three biological replicates ± s.d., overlaid with the original data points. **f**, Dose responses in engineered cells expressing the GEMS with the dual-drug-controlled (venetoclax, A-1155463) switch. Each data point represents the mean ± s.d. of three replicates and the EC_{50} values of the ON phase and IC_{50} values of the OFF phase were calculated using four-parameter nonlinear regression.

pro-apoptotic proteins[16–18] (Supplementary Fig. 1a). Bcl2 and BclXL promote cell survival and are frequently upregulated in many tumors[19–21], making them attractive targets for anticancer drug development. Over the past decades, a number of drugs have been developed. One such drug is navitoclax[22], an experimental, orally active anticancer agent that binds both BclXL and Bcl2. In contrast, venetoclax[23] stands out as the first-in-class (BH3 mimetic) clinically approved drug that selectively binds to Bcl2. A-1155463 (ref. 24) is an experimental drug that has been identified as a selective inhibitor specifically targeting BclXL (Supplementary Fig. 1b). Moreover, a computationally designed binder, LD3, presented a stabilized conformation of the BH3 domain that can bind to both BclXL and Bcl2 (ref. 5) (Supplementary Fig. 1c). For these reasons, we chose BclXL and Bcl2 as the design basis of the drug receptors for our CBP constructs.

In the first step, we sought to construct a dual-drug-controlled switch to test whether the ON and OFF switching processes can be combined in our receptor architecture. We used Bcl2 and BclXL as the orthogonal drug receptors, which interact with the LD3 protein and respond to their own specific inhibitors. In such a setting, the dual-drug-controlled switch will turn ON in response to one drug and OFF in response to the other, thus mimicking bandpass filtering behavior (Supplementary Fig. 1d). The compound A-1155463 interacts with BclXL with a K_d lower than 10 pM, while its binding to Bcl2 is more than 7,000-fold weaker[24]. We confirmed that A-1155463 prevents BclXL from binding to LD3 with a half-maximum inhibitory concentration (IC_{50}) of 106 nM, and does not affect the Bcl2–LD3 interaction, with a detectable IC_{50} in a surface plasmon resonance (SPR) drug competition assay (Fig. 2a). This result shows that Bcl2 is not affected by the inhibitor of BclXL. Thus, we constructed the first dual-drug-controlled switch using Bcl2 and the fused BclXL–LD3 complex, which is expected to turn ON with A-1155463 and to turn OFF with venetoclax. To test the switch behavior, we employed the generalizable extracellular molecule sensor (GEMS) platform[25], which senses extracellular molecules and thus regulates cell surface signaling pathways (Fig. 2a). This receptor

https://doi.org/10.1038/s41589-023-01463-7

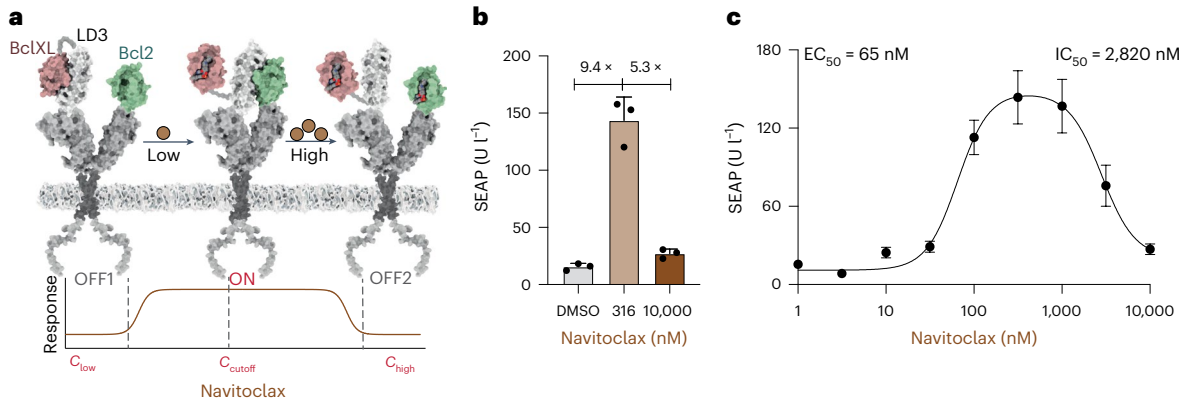

Fig. 3 | Schematic representation and characterization of CBP_{navi}. a, Scheme of CBP_{navi} and its response to different drug concentrations. **b**, Fold change in reporter gene expression between no drug treatment (DMSO; OFF1) versus 316 nM (ON) versus high concentration 10,000 nM (OFF2), 24 h after drug addition. Each bar represents the mean of three biological replicates ± s.d., overlaid with a scatter dot plot of the original data points. **c**, Dose response to navitoclax in engineered cells expressing CBP_{navi}. Each data point represents the mean ± s.d. of three biological replicates. EC_{50} of the ON phase and IC_{50} of the OFF phase were calculated using four-parameter nonlinear regression.

platform is based on a mutated EpoR extracellular and transmembrane domain fused to an IL-6RB intracellular domain. Dimerization of EpoR extracellular domains is controlled by N-terminally fused inducible dimerization domains, which drive IL-6RB activation and STAT3 signaling. The Bcl2 and BclXL–LD3 complexes were fused to the extracellular EpoR domains. The intramolecular interaction of BclXL–LD3 can be disrupted by A-1155463, opening up the binding site of LD3 for Bcl2 protein. The dimerization of Bcl2 and LD3 causes EpoR extracellular domain dimerization and triggers JAK/STAT3 signaling. Active STAT3 drives the expression of a reporter protein (secreted alkaline phosphatase (SEAP)) controlled by a STAT3-dependent promoter. The GEMS with the dual-drug-controlled (A-1155463, venetoclax) switch turned on reporter gene expression with a 100-fold increase in the presence of 100 nM A-1155463, and was effectively shut down by adding 1 µM venetoclax (Fig. 2b). The dual use of A-1155463 and venetoclax showed a slight effect on reporter gene production (Supplementary Fig. 2b) but not on cell proliferation (Supplementary Fig. 2c). The dose response had a half-maximum effective concentration (EC_{50}) of 23 nM in the ON phase and an IC_{50} of 11 nM in the OFF phase (Fig. 2c).

We constructed the second dual-drug-controlled switch using BclXL and Bcl2–LD3 complex, which can be turned ON by venetoclax and turned OFF by A-1155463 (Fig. 2d). Venetoclax selectively binds to Bcl2 rather than to BclXL, with 500-fold stronger affinity[23]. Venetoclax also shows great selectivity in inhibiting the LD3–Bcl2 interaction (IC_{50} = 67 nM) while not affecting the BclXL–LD3 interaction (Supplementary Fig. 2d). These GEMS with dual-drug-controlled (venetoclax, A-1155463) switch showed a close to tenfold increase and decrease in the ON and OFF phases, respectively (Fig. 2e). The dose response had an EC_{50} of 39 nM in the venetoclax-controlled ON phase and an IC_{50} of 103 nM in the A-1155463-controlled OFF phase (Fig. 2f). The combined use of A-1155463 and venetoclax did not cause cellular toxicity on cell proliferation, but a small decrease in reporter protein production was observed (Supplementary Fig. 2e,f).

These results show that the dual-drug-controlled switches can regulate cell surface receptor signaling in an OFF-ON-OFF pattern in response to two drugs, serving as a proof of concept for our design strategy.

A bandpass filter responsive to one chemical input

To test whether the OFF-ON-OFF strategy translated into a single chemical input CBP design, we tested both dual-drug-controlled switches with the Bcl2 family inhibitor navitoclax, which binds to BclXL and Bcl2 with different potencies[22]. We compared navitoclax BclXL–LD3 or Bcl2–LD3 complex disruption in the GEMS platform individually, which showed approximately 4.4-fold more potent activity to BclXL than to Bcl2, and IC_{50} values of 403 nM and 1,773 nM, respectively (Supplementary Fig. 3a,b).

Next, we tested a CBP responsive to navitoclax (CBP_{navi}), which dissociates LD3 from the fused BclXL–LD3 complex to interact with Bcl2 at low concentrations, and dissociates LD3 from Bcl2 at high concentrations (Fig. 3a). CBP_{navi} was used to control receptor activity in the GEMS platform, which can be maximally activated at a cutoff concentration of 320 nM with an approximately ninefold increase in reporter gene expression, and can be turned OFF at 10 µM (Fig. 3b), which does not interfere with reporter gene expression or cell proliferation (Supplementary Fig. 3c,d). We also characterized the ON and OFF kinetics of CBP_{navi}, showing an EC_{50} of 65 nM in the ON phase and an IC_{50} of 2,820 nM in the OFF phase (Fig. 3c).

The CBP_{navi} was constructed on the basis of the different drug sensitivities between BclXL and Bcl2 towards navitoclax, implying that rational design of drug receptors with different drug sensitivities can lead to a general strategy for the engineering of bandpass filter protein devices.

Rational design of CBPs

To rationally design a CBP responding to a chemical input, we used BclXL as the $drug_{low}$ receptor, LD3 as the designed binder and a designed BclXL variant as the $drug_{high}$ receptor (referred to as $BclXL_{high}$) to construct a CBP responsive to BclXL inhibitors (Fig. 4a). To design $BclXL_{high}$, we used a multistate design computational protocol described elsewhere[26] (Methods) and generated six variants, $BclXL_{high}$-v(1–6), which retain binding to LD3 but have higher resistance to A-1155463 (Fig. 4b and Supplementary Table 1). We screened the candidate receptors in the CBP architecture and we observed that $BclXL_{high}$-v(4–6) maintained strong resistance to A-1155463, while $BclXL_{high}$-v(1–3) showed a notable decrease when the drug concentration reached 1 µM (Supplementary Fig. 4a). Thus, $BclXL_{high}$-v(1–3) were chosen as the functional $drug_{high}$ receptors, resulting in three A-1155463-controlled CBPs (referred to as CBP_{A11}-v(1–3)) (Fig. 4c–e). A-1155463 does not perturb reporter gene expression or cell survival at the highest concentration of 10 µM (Supplementary Fig. 4b,c).

All CBP_{A11}-v(1–3) showed distinctive ON phases and OFF phases in response to different concentration ranges of A-1155463. CBP_{A11}-v1 and CBP_{A11}-v3 showed an ON phase with a $Fold_{ON}$ of 70-fold and 26-fold reporter expression over OFF1, respectively; however, they did not efficiently shut down in the OFF2 phase (Fig. 4c,e). CBP_{A11}-v2 demonstrated

https://doi.org/10.1038/s41589-023-01463-7

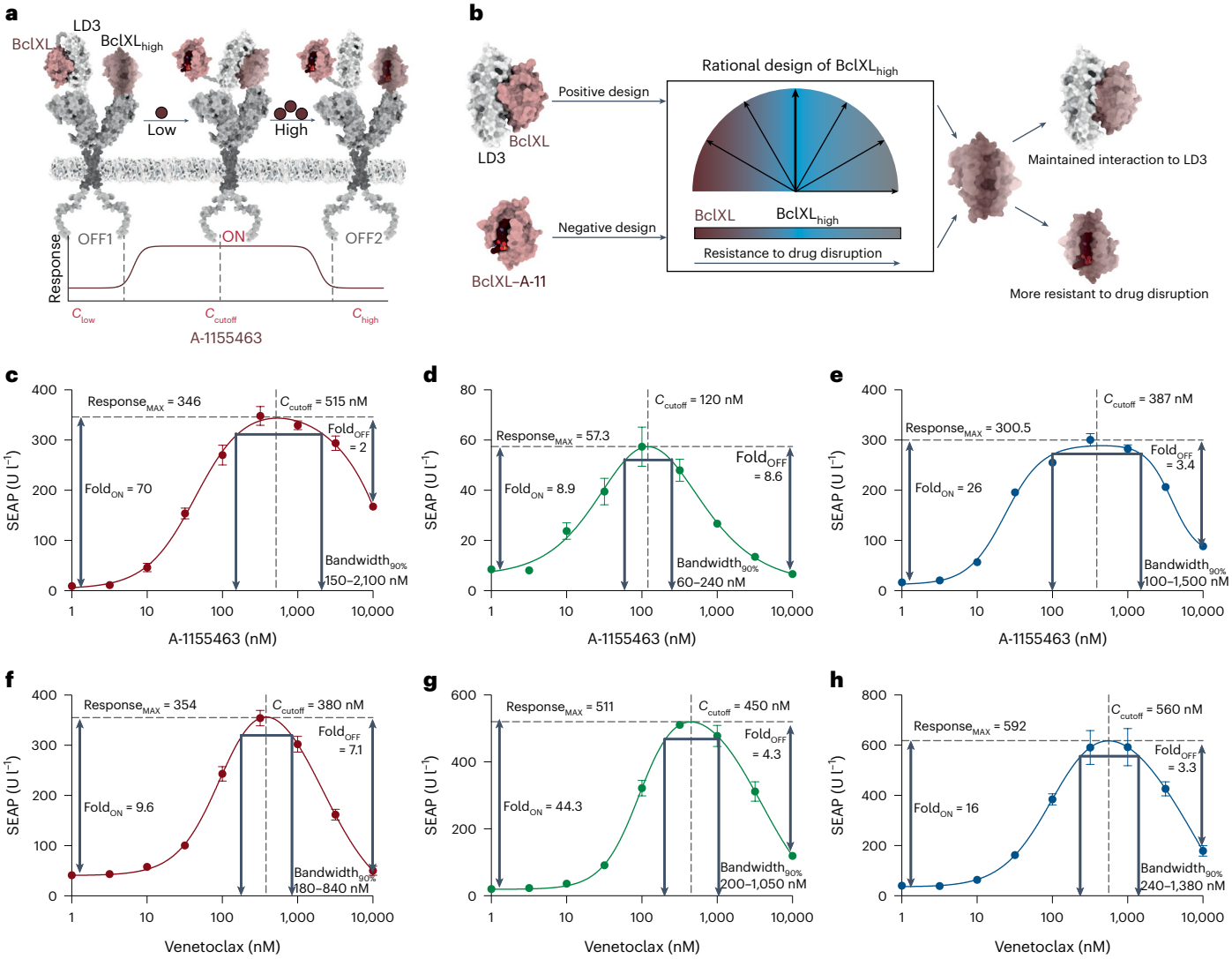

Fig. 4 | Rational design of CBPs that respond to small-molecule drugs. **a**, Scheme of CBP$_{A11}$ and its response in different ranges of drug concentration. **b**, BclXL$_{high}$ designs were generated to perform bandpass filtering functions in response to different concentrations of A-1155463. **c**–**e**, Dose responses of CBP$_{A11}$-v1 (**c**, red), CBP$_{A11}$-v2 (**d**, green) and CBP$_{A11}$-v3 (**e**, blue) in engineered cells. Each data point represents the mean ± s.d. of three replicates and the curves were calculated using bell-shaped fitting. **f**–**h**, Dose responses of CBP$_{vene}$-v1 (**f**, red), CBP$_{vene}$-v2 (**g**, green) and CBP$_{vene}$-v3 (**h**, blue) in engineered cells. Each data point represents the mean ± s.d. of three replicates and the curves were calculated using bell-shaped fitting.

Fold$_{ON}$ of ninefold with 100 nM A-1155463, but shut down to background level at 10 µM (Fig. 4d). We hypothesize that the fold changes (Fold$_{ON}$ and Fold$_{OFF}$) are related to the binding affinities between the drug$_{high}$ receptor and the LD3 protein (BclXL$_{high}$-v1: 44 nM and BclXL$_{high}$-v3: 37 nM versus BclXL$_{high}$-v2: 159 nM), with the stronger binder contributing to the higher Fold$_{ON}$ and lower Fold$_{OFF}$ (Supplementary Fig. 4d). The tighter interaction of BclXL$_{high}$-v1–LD3 and BclXL$_{high}$-v3–LD3 requires a higher drug concentration to dissociate the intermolecular interaction, resulting in a stronger activation and an ineffective disruption in OFF2 phases. Conversely, the weak interaction between BclXL$_{high}$-v2 and LD3 resulted in a lower receptor activation but complete disruption in the OFF phase of CBP$_{A11}$-v2 (Fig. 4d).

Next, we characterized the cutoff concentration (C_{cutoff}) and bandwidth (Bandwidth$_{90\%}$) parameters of CBP$_{A11}$-v(1–3). CBP$_{A11}$-v2 showed the lowest C_{cutoff} at around 120 nM, and CBP$_{A11}$-v1 and CBP$_{A11}$-v3 both have a C_{cutoff} above 300 nM (Fig. 4c–e). CBP$_{A11}$-v2 has the narrowest Bandwidth$_{90\%}$ of 80–240 nM. In contrast, CBP$_{A11}$-v1 has a Bandwidth$_{90\%}$ of 150 nM to 2,100 nM (Fig. 4c–e). These data show that the drug sensitivity of BclXL$_{high}$-v(1–3) to A-1155463 (Supplementary Fig. 4e) is well translated into the differences in the C_{cutoff} and Bandwidth$_{90\%}$ of CBP$_{A11}$-v(1–3). The more sensitive BclXL$_{high}$ compared to wild-type BclXL, the lower the C_{cutoff} and Response$_{MAX}$, and the narrower the Bandwidth$_{90\%}$. For instance, BclXL$_{high}$-v1 has the strongest drug resistance to A-1155463, which showed a correspondingly high C_{cutoff} and the widest Bandwidth$_{90\%}$.

Next, we constructed a venetoclax (Federal Drug Administration-approved Bcl2 inhibitor) responsive CBP (CBP$_{vene}$) using Bcl2, LD3 and a designed drug$_{high}$ receptor based on Bcl2 (Bcl2$_{high}$) (Supplementary Fig. 5a). Using multistate design, we generated eight Bcl2$_{high}$ variants (referred to as Bcl2$_{high}$-v(1–8)), which were designed for lower affinity to venetoclax compared to native Bcl2 (Supplementary Fig. 5b and Supplementary Table 2). CBP constructs including Bcl2$_{high}$-v(1–8) were screened, and Bcl2$_{high}$-v2, Bcl2$_{high}$-v4 and Bcl2$_{high}$-v5 presented the desired behavior, with a sharp decrease when venetoclax exceeds 100 nM (Supplementary Fig. 5c). We confirmed that 10 µM venetoclax is not toxic for reporter gene expression and cell proliferation (Supplementary Fig. 5d,e).

CBP$_{vene}$-v2 showed a Fold$_{ON}$ and a Fold$_{OFF}$ of about ninefold (Fig. 4f). CBP$_{vene}$-v4 has a higher Fold$_{ON}$ (44-fold) but does not completely shut

https://doi.org/10.1038/s41589-023-01463-7

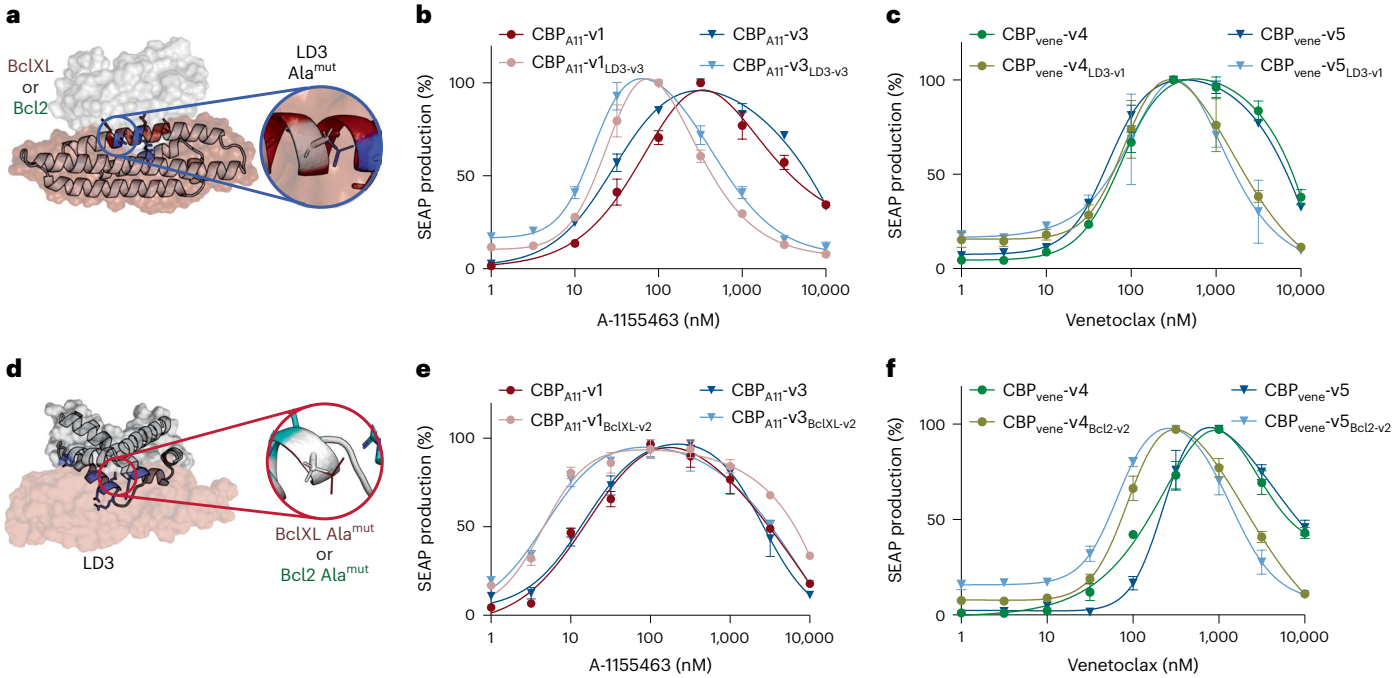

Fig. 5 | Rational tuning of binding affinities between the LD3 binder and drug receptors can further modulate the characteristics of CBPs. a, Rational tuning of binding affinities between LD3 (in red) and the drug receptor (BclXL or Bcl2 in white surface). Positions were selected and mutated to alanine (Ala^{mut}) on LD3 to decrease the binding affinity. **b**, Normalized dose responses of CBP_{A11}-v1 and CBP_{A11}-v3 with and without LD3-v3. **c**, Normalized dose responses of CBP_{vene}-v4 and CBP_{vene}-v5 with and without LD3-v1. **d**, Scheme of the rational tuning of binding affinities between LD3 and the drug receptor by alanine scanning on BclXL or Bcl2 proteins. **e**, Normalized drug dose-dependent responses of CBP_{A11}-v1 (red) and CBP_{A11}-v3 (blue) compared with CBP_{A11}-$v1_{BclXL\text{-}v2}$ (pink) and CBP_{A11}-$v3_{BclXL\text{-}v2}$ (turquoise) in engineered cells. **f**, Normalized drug dose-dependent responses of CBP_{vene}-v4 (green) and CBP_{vene}-v5 (blue) compared with CBP_{vene}-$v4_{Bcl2\text{-}v2}$ (asparagus) and CBP_{vene}-$v5_{Bcl2\text{-}v2}$ (turquoise) in engineered cells. In **b**, **c**, **e** and **f** each data point represents the mean ± s.d. of three replicates and the curves were computed using bell-shaped fitting.

off at 10 μM, with a $Fold_{OFF}$ of 3.4 (Fig. 4g). CBP_{vene}-v5 displayed a $Fold_{ON}$ of 16-fold, the highest C_{cutoff} at 560 nM and the widest $Bandwidth_{90\%}$, with a range of 240–1,380 nM (Fig. 4h). Notably, the binding affinities between $Bcl2_{high}$-v(2,4,5) and LD3 are close (Supplementary Fig. 6a), indicating that their drug resistance is critical for regulating the C_{cutoff} and $Bandwidth_{90\%}$. For instance, the $Bcl2_{high}$-v4 is more resistant than $Bcl2_{high}$-v2 (Supplementary Fig. 6b), leading to the higher C_{cutoff} (CBP_{vene}-v4: 450 nM versus CBP_{vene}-v2: 380 nM) and the wider $Bandwidth_{90\%}$ (CBP_{vene}-v4: 200–1,050 nM versus CBP_{vene}-v2: 180–840 nM).

We developed CBPs controlled by BclXL and Bcl2 inhibitors by rationally designing $drug_{high}$ receptors with reduced drug sensitivities and using a multidomain architecture that can provide output analogous to bandpass filters.

Tuning CBPs towards lower drug demand and larger bandwidth

We observed that CBP_{A11}-v1 and CBP_{A11}-v3, or CBP_{vene}-v4 and CBP_{vene}-v5, cannot be fully turned off at the highest drug concentration of 10 μM. However, very high drug concentrations may cause unwanted side effects due to toxicity. To improve the performance of these CBPs, we tuned the binding affinities between LD3 and the two drug receptors to lower their C_{cutoff} and increase the shut-down efficiency.

Previously, we showed that mutations in the binding region of LD3 weaken the interaction of BclXL–LD3, thus lowering the drug demand to dissociate BclXL–LD3 (ref. 26) (Fig. 5a). We expect to obtain the same effect of such mutations in the context of the CBPs, to lower drug concentrations to turn ON and shut OFF the CBPs. We replaced LD3 in CBP_{A11}-v(1–3) with LD3-v(1–3) to test whether they respond to lower concentrations of A-1155463. LD3-v3-based designs successfully shifted the C_{cutoff} of all three CBP_{A11}-v(1–3) to lower drug concentrations (Supplementary Table 3 and Supplementary Fig. 7a–c). CBP_{A11}-$v1_{LD3\text{-}v3}$ and CBP_{A11}-$v3_{LD3\text{-}v3}$ were the best performers in terms of fold change, and both shifted their C_{cutoff} from above 500 nM to below 100 nM, and effectively shut down at 10 μM (Fig. 5b). However, the new LD3-v3-based CBPs also showed a lower level of ON response (Supplementary Fig. 7d,e).

We also replaced LD3 with LD3-v(1–3) in CBP_{vene}-v(2,4,5) to test whether they respond to lower concentration of venetoclax. Unlike CBP_{A11}-v(1–3), LD3-v3 replacement in CBP_{vene}-v(2,4,5) showed leaky background activities, which failed to maintain the bandpass filtering behavior (Supplementary Fig. 8a–c). The LD3-v1 replacement shifted both CBP_{vene}-$v4_{LD3\text{-}v1}$ and CBP_{vene}-$v5_{LD3\text{-}v1}$ to lower drug concentration ranges, with no notable decrease in C_{cutoff} values compared to CBP_{vene}-v4 or CBP_{vene}-v5, respectively (Fig. 5c and Supplementary Fig. 8d,e). We found that the binding affinity of the LD3-v3–BclXL complex in CBP_{A11}-$v1_{LD3\text{-}v3}$ and CBP_{A11}-$v3_{LD3\text{-}v3}$ is 5,000-fold weaker compared to the wild-type LD3–BclXL complex[26], which can drastically lower the C_{cutoff} of CBP_{A11}-v1 and CBP_{A11}-v3. However, the binding affinity of LD3-v1–Bcl2 in CBP_{vene}-$v4_{LD3\text{-}v1}$ and CBP_{vene}-$v5_{LD3\text{-}v1}$ is less than 200-fold weaker than LD3–Bcl2 (ref. 26), which was not capable of shifting the C_{cutoff} values substantially. We confirmed that the tuning of LD3 led to adjustment of the response of CBP_{A11} and CBP_{vene} to lower drug concentrations.

Next, we tested whether we could engineer the $drug_{low}$ receptor to increase the sensitivity of the OFF1 to ON regulatory phase (Fig. 5d). Since the switch from ON to OFF2 should not be affected, we hypothesized that this strategy could also increase bandwidth. We scanned residues at the interface of the BclXL–LD3 complex, selected three residues on BclXL and mutated them individually to alanine (Methods and Supplementary Table 4). Among the BclXL variants (referred to as BclXL-v(1–3)), BclXL-v2 emerged as the best candidate, since BclXL-v1 and BclXL-v3 failed to function as bandpass filters in a CBP_{A11} setting

(Supplementary Fig. 9a–c). We found that both CBP_{A11}-$v1_{BclXL\text{-}v2}$ and CBP_{A11}-$v3_{BclXL\text{-}v2}$ showed similar C_{cutoff} values and a wider bandwidth compared to CBP_{A11}-v1 and CBP_{A11}-v3, respectively (Fig. 5e). While OFF-phase kinetics remained similar, CBP_{A11}-$v1_{BclXL\text{-}v2}$ and CBP_{A11}-$v3_{BclXL\text{-}v2}$ turned ON at lower drug concentrations than CBP_{A11}-v1 and CBP_{A11}-v3, reflecting the weaker interaction of BclXL-v2–LD3 than BclXL–LD3 (Supplementary Fig. 9d,e).

Applying the same principle to CBP_{vene}-v(2,4,5), we introduced alanine mutations into Bcl2 (Methods and Supplementary Table 5), referred to as Bcl2-v(1–6). On the basis of the screening results (Supplementary Fig. 10a–c), Bcl2-v2 was used for constructing CBP_{vene}-$v4_{Bcl2\text{-}v2}$ and CBP_{vene}-$v5_{Bcl2\text{-}v2}$, which demonstrated a lower C_{cutoff} and unexpectedly also shut down in lower concentrations compared to CBP_{vene}-v4 and CBP_{vene}-v5, respectively (Fig. 5f and Supplementary Fig. 10d,e).

Altogether, we showed improved performance of CBP_{A11} and CBP_{vene}, with better $Fold_{OFF}$ values and lower C_{cutoff} values, by rationally tuning the binding affinities between LD3 and the two drug receptors. We also redesigned the $drug_{low}$ receptors of CBP_{A11} and CBP_{vene}, BclXL and Bcl2, respectively, which shifted the ON regulatory phase to lower drug concentration ranges to tune the bandwidth and C_{cutoff} values of CBPs.

Discussion

In contrast to electrical devices, cells as biological computing units use chemical inputs and biological molecules for signal processing. Protein switches have been designed to turn cellular activity ON or OFF; however, protein modules that perform bandpass filter behavior independent of engineered transcription factors remain unexplored. Here, we use computational protein design to develop protein-based bandpass filters with tunable behavior that detect drug concentrations and regulate cellular activities in an OFF-ON-OFF pattern.

First, we mimicked the behavior of bandpass filters by combining two drugs as ON and OFF signals. This approach has been attempted using engineered bacterial transcription factors to respond to two chemicals[12]; however, it lacks transferability when different transcription factors or controlled genetic circuits are required. We presented a new strategy to engineer protein-based bandpass filters by rationally designing a $drug_{high}$ receptor that remains bound to the designed binder (ON) and can only be dissociated at high drug concentrations (OFF). In this way, each CBP responds to a single chemical input and senses the ON and OFF signals dependent on the chemical concentrations. In total, we designed ten CBPs based on BclXL and Bcl2 inhibitors producing different cutoff concentrations, from below 100 nM (for example, CBP_{A11}-$v1_{LD3\text{-}v3}$) to above 500 nM (for example, CBP_{vene}-v5), as well as regulatory bandwidths with different ranges (for example, 60–240 nM for CBP_{A11}-v2 versus 100–1,500 nM for CBP_{A11}-v3). By rationally mutating the designed binder (LD3), CBPs can be tuned to perform with higher drug sensitivity in the trade-off with maximal response. We also demonstrated that by modulating different drug sensitivities of $drug_{low}$ receptors, the greater the difference in drug sensitivity between $drug_{high}$ receptor and $drug_{low}$ receptor, the larger the bandwidth. These results demonstrate that rational protein design can be used to design and tune CBPs.

Protein-based CBPs function by induced protein–protein interactions, which can be modular and less restricted than intracellular genetic circuit-based bandpass filters[27]. While previous synthetic bandpass filter systems sensed small molecules and produced a transcriptional response[8,12,15], they did not enable the control of other cell functions, such as signaling pathways. We utilized the designed CBPs to control engineered cytokine receptors that detect extracellular signals and regulate intracellular JAK/STAT3 signaling pathways. This application demonstrated the potential of CBPs in receptor engineering for sensing external cues, which is a first step towards sensing peptide or protein targets with bandpass behavior. Such systems could ultimately lead to the integration of bandpass filters into engineered cell communication networks for synthetic morphology or other autonomously controlled cell consortia[28,29].

CBP-regulated systems have defined ranges of drug concentrations to sustain specific activity levels, in contrast to the simpler ON/OFF protein switch-based systems. For instance, the CBP_{A11}-v1 can sustain 90% of receptor activation within drug concentrations from 150 nM to 2.1 µM. As a possible safety feature, exceeding the cutoff concentration could serve as a negative feedback to tune down the output in potential therapeutic applications. This drug concentration-dependent pattern of CBPs can be applied in controlling biological or therapeutic activities that require self-regulatory feedback from their inputs. We envision that the CBPs will be valuable components to control signal processing and to engineer sophisticated cellular functions.

Online content

Any methods, additional references, Nature Portfolio reporting summaries, source data, extended data, supplementary information, acknowledgements, peer review information; details of author contributions and competing interests; and statements of data and code availability are available at https://doi.org/10.1038/s41589-023-01463-7.

References

1. Basu, S., Karig, D. & Weiss, R. in *DNA Computing* Vol. 2568 (eds. Hagiya, M. & Ohuchi, A.) 61–72 (Springer, 2003).
2. Wang, Y.-H., Wei, K. Y. & Smolke, C. D. Synthetic biology: advancing the design of diverse genetic systems. *Annu. Rev. Chem. Biomol. Eng.* **4**, 69–102 (2013).
3. Stein, V. & Alexandrov, K. Synthetic protein switches: design principles and applications. *Trends Biotechnol.* **33**, 101–110 (2015).
4. Clackson, T. et al. Redesigning an FKBP-ligand interface to generate chemical dimerizers with novel specificity. *Proc. Natl Acad. Sci. USA* **95**, 10437–10442 (1998).
5. Giordano-Attianese, G. et al. A computationally designed chimeric antigen receptor provides a small-molecule safety switch for T-cell therapy. *Nat. Biotechnol.* **38**, 426–432 (2020).
6. Ausländer, D. et al. Programmable full-adder computations in communicating three-dimensional cell cultures. *Nat. Methods* **15**, 57–60 (2018).
7. Christian, J. L. Morphogen gradients in development: from form to function. *WIREs Dev. Biol.* **1**, 3–15 (2012).
8. Basu, S., Gerchman, Y., Collins, C. H., Arnold, F. H. & Weiss, R. A synthetic multicellular system for programmed pattern formation. *Nature* **434**, 1130–1134 (2005).
9. Sohka, T. et al. An externally tunable bacterial band-pass filter. *Proc. Natl Acad. Sci. USA* **106**, 10135–10140 (2009).
10. Sohka, T., Heins, R. A. & Ostermeier, M. Morphogen-defined patterning of *Escherichia coli* enabled by an externally tunable band-pass filter. *J. Biol. Eng.* **3**, 10 (2009).
11. Brechun, K. E., Arndt, K. M. & Woolley, G. A. Selection of protein–protein interactions of desired affinities with a bandpass circuit. *J. Mol. Biol.* **431**, 391–400 (2019).
12. Groseclose, T. M., Hersey, A. N., Huang, B. D., Realff, M. J. & Wilson, C. J. Biological signal processing filters via engineering allosteric transcription factors. *Proc. Natl Acad. Sci. USA* **118**, e2111450118 (2021).
13. Huynh, L., Kececioglu, J., Köppe, M. & Tagkopoulos, I. Automatic design of synthetic gene circuits through mixed integer non-linear programming. *PLoS One* **7**, e35529 (2012).
14. Kong, W., Blanchard, A. E., Liao, C. & Lu, T. Engineering robust and tunable spatial structures with synthetic gene circuits. *Nucleic Acids Res.* **45**, 1005–1014 (2017).
15. Greber, D. & Fussenegger, M. An engineered mammalian band-pass network. *Nucleic Acids Res.* **38**, e174 (2010).

16. Shamas-Din, A., Kale, J., Leber, B. & Andrews, D. W. Mechanisms of action of Bcl-2 family proteins. *Cold Spring Harb. Perspect. Biol.* **5**, a008714 (2013).
17. Hanada, M., Aimé-Sempé, C., Sato, T. & Reed, J. C. Structure-function analysis of Bcl-2 protein. Identification of conserved domains important for homodimerization with Bcl-2 and heterodimerization with Bax. *J. Biol. Chem.* **270**, 11962–11969 (1995).
18. Pawlowski, J. & Kraft, A. S. Bax-induced apoptotic cell death. *Proc. Natl Acad. Sci. USA* **97**, 529–531 (2000).
19. Campbell, K. J. & Tait, S. W. G. Targeting BCL-2 regulated apoptosis in cancer. *Open Biol.* **8**, 180002 (2018).
20. Roberts, A. W. et al. Targeting BCL2 with venetoclax in relapsed chronic lymphocytic leukemia. *N. Engl. J. Med.* **374**, 311–322 (2016).
21. Qian, S. et al. The role of BCL-2 family proteins in regulating apoptosis and cancer therapy. *Front. Oncol.* **12**, 985363 (2022).
22. Tse, C. et al. ABT-263: a potent and orally bioavailable Bcl-2 family inhibitor. *Cancer Res.* **68**, 3421–3428 (2008).
23. Souers, A. J. et al. ABT-199, a potent and selective BCL-2 inhibitor, achieves antitumor activity while sparing platelets. *Nat. Med.* **19**, 202–208 (2013).
24. Tao, Z.-F. et al. Discovery of a potent and selective BCL-X_L inhibitor with in vivo activity. *ACS Med. Chem. Lett.* **5**, 1088–1093 (2014).
25. Scheller, L., Strittmatter, T., Fuchs, D., Bojar, D. & Fussenegger, M. Generalized extracellular molecule sensor platform for programming cellular behavior. *Nat. Chem. Biol.* **14**, 723–729 (2018).
26. Shui, S. et al. A rational blueprint for the design of chemically-controlled protein switches. *Nat. Commun.* **12**, 5754 (2021).
27. Gao, X. J., Chong, L. S., Kim, M. S. & Elowitz, M. B. Programmable protein circuits in living cells. *Science* **361**, 1252–1258 (2018).
28. Ho, C. & Morsut, L. Novel synthetic biology approaches for developmental systems. *Stem Cell Rep.* **16**, 1051–1064 (2021).
29. Pistikou, A.-M. M. et al. Engineering a scalable and orthogonal platform for synthetic communication in mammalian cells. Preprint at *bioRxiv* https://doi.org/10.1101/2023.01.18.524631 (2023).

Methods

Multistate design of single-drug reversible BclXL and Bcl2

As reported previously, a set of residues in the receptor protein (BclXL/Bcl2) binding site was selected for redesign[26]. From this set, a number of mutations were evaluated for binding energy to the binder protein (LD3) (positive design) or the drug (negative design). Afterwards, all mutations were ranked according to the difference in energy between the positive design and the negative design. The structure of BclXL bound to A-1155463 (PDB 4QVX) was used for the negative design strategy, while the model of BclXL bound to LD3 (based on the BclXL–BIM BH3 structure with PDB 3FDL) was used for positive design. Six BclXL residues in the binding site of A-1155463 (E98, R102, F105, T109, S145 and A149) were manually selected for redesign due to their proximity to drug moieties and relative distance to LD3 in the positive design structure. Each of these residues was allowed to mutate to residues with similar size/properties, restricted to a maximum of two simultaneous mutations from wild type: E98: {E/S}, R102: {F/R/K/D/E/H}, F105: {F/L/V/I/A}; T109: {S/A/T/L/V}; S145: {S/D/E/V/A}; A149: {V/A/L/I}. Six sequences, $BclXL_{high}$-v1 (T109L, A149L), $BclXL_{high}$-v2 (A149V), $BclXL_{high}$-v3 (R102F, T109V), $BclXL_{high}$-v4 (E98S,R102E, F105I), $BclXL_{high}$-v5 (R102E, F105I, T109L) and $BclXL_{high}$-v6 (E98S, R102E, F105I, T109L), were generated to test for single-drug reversible BclXL. All sequences are listed in Supplementary Table 1.

The structure of Bcl2 bound to venetoclax (PDB 6O0K) was used for the negative design strategy, while the model of Bcl2 bound to LD3 (PDB 6IWB) was used for positive design. Five Bcl2 residues in the binding site of venetoclax (A100, D103, V148, V156 and Y202) were manually selected for redesign due to their closeness to drug moieties and relative distance to LD3 in the positive design structure. Each of these residues was allowed to mutate to amino acids with similar size/properties, restricted to a maximum of two simultaneous mutations from wild type: A100: {A/S/T/V}, D103: {D/N/E/Q/S}, V148: {V/I/L/M/T}, V156: {V/I/L/M/T} and Y202: {Y/W/F/H/R/K/Q/E}. Three sequences, srBcl2-v1(V156I, Y202H), srBcl2-v2(D103N, Y202H) and srBcl2-v3(A100T, D103S), were selected from the top results. Five sequences were generated based on the observation of venetoclax resistance in clinical trials where G101V occurs alone or together with D103Y and D103E. Hence, we constructed srBcl2-v4(G101V), srBcl2-v5(D103Y), srBcl2-v6(G101V,D103Y), srBcl2-v7(D103E) and srBcl2-v8(G101V,D103E). All sequences are listed in Supplementary Table 2.

AlaScan on LD3 and drug receptor proteins

LD3-v(1–3) variants were designed previously[26] and sequences of LD3-v(1–3) are listed in Supplementary Table 3. The BclXL protein in complex with LD3 was computationally redesigned for a range of decreasing binding affinities. Rosetta's alanine scanning filter was used to evaluate the change in $\Delta\Delta G$ for the LD3–BclXL complex (PDB 3FDL) upon mutating each of the 22 residues in the interface of BclXL to alanine. The resulting list was then sorted by the change in $\Delta\Delta G$, and three residues with positive levels of change in $\Delta\Delta G$ were selected: Q90 (0.33 REU), L90 (1.17 REU) and R99 (4.78 REU), where higher Rosetta energy unit (REU) values are predicted to result in greater affinity losses. The three mutations were selected to provide a 'gradient' of affinities between LD3 and BclXL; sequences of BclXL-v(1–3) are listed in Supplementary Table 4. By the same principle, Rosetta's alanine scanning filter was used to evaluate the change in $\Delta\Delta G$ for the LD3–Bcl2 complex (PDB 6IWB) upon mutating each of the 32 residues in the interface of BclXL to alanine. The resulting list was then sorted by the change in $\Delta\Delta G$, and six residues with positive levels of change in $\Delta\Delta G$ were selected: F63 (6.29 REU), V92 (1.29 REU), E95 (1.50 REU), L96 (0.88 REU), R105 (1.52 REU) and E111 (0.59 REU), where higher REU values are predicted to result in greater affinity losses. The six mutations were selected to provide a 'gradient' of affinities between LD3 and Bcl2; sequences of Bcl2-v(1–6) are listed in Supplementary Table 5.

SPR assay for protein–protein binding affinities

SPR measurements were performed on a Biacore 8K device (GE Healthcare). The mutual designed binder (LD3) was immobilized on a CM5 chip (GE Life Science) as a ligand with the concentration at 5 μg ml^{-1} for 120 s contact time in pH 4.5 sodium acetate solutions. Serial dilutions of the analytes (BclXL or Bcl2 and their variants) in HBS-EP buffer (10 mM HEPES, 150 mM NaCl, 3 mM EDTA and 0.005% surfactant P20; GE Life Science) were flowed over the immobilized chips. After each injection cycle, surface regeneration was performed using 10 mM NaOH (pH 11.95). Affinities (K_d) were obtained using a steady binding model of the equilibrium model with Biacore 8K evaluation software.

SPR drug competition assay

Drug IC_{50} values for disrupting heterodimers were measured on a Biacore 8K device. A 5 μM portion of analyte was mixed with 10 μM of BclXL or Bcl2 inhibitors according to the analyte. The mixtures of analyte and drug were injected onto the LD3 immobilized channel.

Compounds

Venetoclax (>99.9%, Chemietek, catalog no. CT-A199), A-1155463 (99.5%, Chemietek, catalog no. CT-A115) and NVP-CGM097 (100% optically pure, Chemietek, catalog no. CT-CGM097) were used directly without further purification. Venetoclax, A-1155463 and NVP-CGM097 were each dissolved in DMSO as 10 mM stocks. Stocks were aliquoted and stored at −20 °C until use.

Cell transfection and drug treatment

HEK293T cells were maintained in DMEM medium (Thermo Fisher) with 10% FBS (Gibco) and pen/strep (Thermo Fisher) at 37 °C and 5% CO_2 in a humidified incubator. Cells were maintained and split every 2 d at around 80% confluence.

HEK293T cells were seeded in a 96-well plate 24 h before transfection. The transfection mix in each well consisted of 3 ng of constitutive human CMV promoter driven mammalian STAT3 expression vector (P_{hCMV}-STAT3-pA), 30 ng of STAT3-induced reporter expression (O_{Stat3}-$P_{hCMVmin}$-SEAP-pA) and 50 ng of expression vectors for each GEMS receptor chain (PSV40-IgK-($drug_{high}$ receptor)-EpoRm-IL-6RBm-pA and PSV40-IgK-($drug_{low}$ receptor-GGGGSX3-LD3)-EpoRm-IL-6RBm-pA). For the specific $drug_{high}$ receptor and $drug_{low}$ receptor used in the different cellular assays, they are indicated as wild type or with mutations. Then, plasmid DNA was mixed with 50 μl opti-MEM (Thermo Fisher) and 600 ng of polyethyleneimine (Polysciences, catalog no. 24765-1). For drug treatment experiments, drugs were added 12 h post-transfection and incubated with cells for 24 h before the SEAP reporter detection assay.

Reporter detection assay

SEAP activity (U l^{-1}) in cell culture supernatants was quantified by kinetic measurements at 405 nm (1 minute per measurement for 30 cycles) of absorbance increase due to phosphatase-mediated hydrolysis of *para*-nitrophenyl phosphate (pNPP). A 4–80 μl portion of supernatant was adjusted with water to a final volume of 80 μl, heat inactivated (30 min at 65 °C) and mixed in a 96-well plate with 100 μl of 2× SEAP buffer (20 mM homoarginine (FluorochemChemie), 1 mM $MgCl_2$, 21% (v/v) diethanolamine (Sigma Aldrich, catalog no. D8885), pH 9.8) and 20 μl of substrate solution containing 20 mM pNPP (Sigma Aldrich, catalog no. 71768).

Statistics

Binding affinities of SPR drug competition assays were calculated using three-parameter nonlinear regression in GraphPad Prism (v.8.3.0). Representative data of cell assays are presented as individual values and mean values (bars). $n = 3$ refers to biological replicates. All IC_{50} or EC_{50} values of cell assays reported were calculated using four-parameter

nonlinear regression ± s.d. Bandpass features of cutoff concentrations and Bandwidth$_{90\%}$ were estimated based on the curve fitted using bell-shaped curve nonlinear regression in GraphPad Prism (v.8.3.0).

Reporting summary

Further information on research design is available in the Nature Portfolio Reporting Summary linked to this article.

Data availability

The data supporting the findings of this study are available within the article and its Supplementary Information. Other data and reagents are available from the corresponding authors upon reasonable request. Source data are provided with this paper.

Acknowledgements

The computational simulations were facilitated by SCITAS at EPFL and by the Swiss National Supercomputer Center. We thank S. Maerkl for initial discussions on the bandpass filter concept. S.S. was supported by Swiss Cancer League grant no. KFS-5032-02-2020. L.S. was supported by grant no. 2021-446 of the Strategic Focus Area 'Personalized Health and Related Technologies (PHRT)' of the ETH Domain and by the Anniversary Foundation of Swiss Life for Public Health and Medical Research. B.E.C. was supported by the Swiss National Science Foundation, the NCCR in Chemical Biology, the NCCR in Molecular Systems Engineering, the Swiss Cancer League grant no. KFS-5032-02-2020 and the ERC Starting grant no. 716058.

Author contributions

S.S., L.S. and B.E.C. conceived the work. S.S. performed the experimental characterization. S.S., L.S. and B.E.C. designed the experiments and analyzed the results. S.S., L.S. and B.E.C. wrote the manuscript.

Competing interests

The authors declare no competing interests.

Additional information

Supplementary information The online version contains supplementary material available at https://doi.org/10.1038/s41589-023-01463-7.

Correspondence and requests for materials should be addressed to Bruno E. Correia.

Peer review information *Nature Chemical Biology* thanks the anonymous reviewers for their contribution to the peer review of this work.

nature portfolio

Corresponding author(s): Bruno Emanuel Correia

Last updated by author(s): 16-09-2022

Reporting Summary

Nature Portfolio wishes to improve the reproducibility of the work that we publish. This form provides structure for consistency and transparency in reporting. For further information on Nature Portfolio policies, see our Editorial Policies and the Editorial Policy Checklist.

Statistics

For all statistical analyses, confirm that the following items are present in the figure legend, table legend, main text, or Methods section.

n/a	Confirmed
☐	☒ The exact sample size (*n*) for each experimental group/condition, given as a discrete number and unit of measurement
☐	☒ A statement on whether measurements were taken from distinct samples or whether the same sample was measured repeatedly
☐	☒ The statistical test(s) used AND whether they are one- or two-sided *Only common tests should be described solely by name; describe more complex techniques in the Methods section.*
☒	☐ A description of all covariates tested
☒	☐ A description of any assumptions or corrections, such as tests of normality and adjustment for multiple comparisons
☐	☒ A full description of the statistical parameters including central tendency (e.g. means) or other basic estimates (e.g. regression coefficient) AND variation (e.g. standard deviation) or associated estimates of uncertainty (e.g. confidence intervals)
☒	☐ For null hypothesis testing, the test statistic (e.g. *F*, *t*, *r*) with confidence intervals, effect sizes, degrees of freedom and *P* value noted *Give P values as exact values whenever suitable.*
☒	☐ For Bayesian analysis, information on the choice of priors and Markov chain Monte Carlo settings
☒	☐ For hierarchical and complex designs, identification of the appropriate level for tests and full reporting of outcomes
☒	☐ Estimates of effect sizes (e.g. Cohen's *d*, Pearson's *r*), indicating how they were calculated

Our web collection on statistics for biologists contains articles on many of the points above.

Software and code

Policy information about availability of computer code

Data collection	Pymol and ChimeraX were used for structural visualization Rosetta was used for protein design. Two rosetta script used in this paper were published before (https://doi.org/10.1038/s41467-021-25735-9)
Data analysis	Graphpad Prism(Version 8.3.0)

For manuscripts utilizing custom algorithms or software that are central to the research but not yet described in published literature, software must be made available to editors and reviewers. We strongly encourage code deposition in a community repository (e.g. GitHub). See the Nature Portfolio guidelines for submitting code & software for further information.

Data

Policy information about availability of data

All manuscripts must include a data availability statement. This statement should provide the following information, where applicable:

- Accession codes, unique identifiers, or web links for publicly available datasets
- A description of any restrictions on data availability
- For clinical datasets or third party data, please ensure that the statement adheres to our policy

The data supporting the findings of this study are available within the article and its Supplementary Information. The codes used in this paper is also published in previous paper (https://doi.org/10.1038/s41467-021-25735-9) and available in github (https://github.com/LPDI-EPFL/CDH_AIR).

Human research participants

Policy information about studies involving human research participants and Sex and Gender in Research.

Reporting on sex and gender	*Use the terms sex (biological attribute) and gender (shaped by social and cultural circumstances) carefully in order to avoid confusing both terms. Indicate if findings apply to only one sex or gender; describe whether sex and gender were considered in study design whether sex and/or gender was determined based on self-reporting or assigned and methods used. Provide in the source data disaggregated sex and gender data where this information has been collected, and consent has been obtained for sharing of individual-level data; provide overall numbers in this Reporting Summary. Please state if this information has not been collected. Report sex- and gender-based analyses where performed, justify reasons for lack of sex- and gender-based analysis.*
Population characteristics	*Describe the covariate-relevant population characteristics of the human research participants (e.g. age, genotypic information, past and current diagnosis and treatment categories). If you filled out the behavioural & social sciences study design questions and have nothing to add here, write "See above."*
Recruitment	*Describe how participants were recruited. Outline any potential self-selection bias or other biases that may be present and how these are likely to impact results.*
Ethics oversight	*Identify the organization(s) that approved the study protocol.*

Note that full information on the approval of the study protocol must also be provided in the manuscript.

Field-specific reporting

Please select the one below that is the best fit for your research. If you are not sure, read the appropriate sections before making your selection.

☒ Life sciences ☐ Behavioural & social sciences ☐ Ecological, evolutionary & environmental sciences

For a reference copy of the document with all sections, see nature.com/documents/nr-reporting-summary-flat.pdf

Life sciences study design

All studies must disclose on these points even when the disclosure is negative.

Sample size	No sample size calculation was performed. For the cell culture experiments, n=3 biological replicates were predicted to be sufficient for estimating the spread of data, for calculating the mean and for detecting statistically significant differences between compared groups. Preliminary results and experience in similar cell culture experiments support n=3 biologically independent samples per individual experiment as sufficient to detect meaningful differences in reporter gene expression.
Data exclusions	We did minimal data exclusion of points where the experiment was technically problematic and the measurements of the reporter proteins yielded negative values. Here is a summary of the excluded data figure 5b (three data points excluded of CBP-A11v1 and CBP-A11v3 measurement, 3 out of 30), figure 5f (three data points excluded of CBPvene-v5, 3 out of 30).
Replication	All cellular experiments were performed with three biological replicates. For reported bandpass curves have been repeated in three independent assays, figure3c, figure 4c-h, figure 5b-c, figure 5e-f.
Randomization	No animal or human research participants were involved. For cell culture experiments, no covariates based on sample allocations to experimental groups could be observed and no randomization was performed. All transfection of drug treated and non-treated, dose-dependent drug treatment were performed with cells transfected under same conditions with the same transfection mix and subsequent addition of drugs. The cells for these experiments were cultured in the same plate with the same well-distribution. For most experiments the inner 60 wells of 96 well plates were used to avoid the effects of evaporation.
Blinding	No animal or human research participants were involved. For cell culture experiments investigators were not blinded. Our workflow makes extensive use of multichannel pipetting for conducting several experiments at the same time. Hence it is unlikely that even subconcious bias regarding anticipated results could influence the data. The parallel conduction of several experiments makes it unlikely that the researcher could identify any given transfection mix, hence elaborate blinding procedures were deemed unnecessary.

Reporting for specific materials, systems and methods

We require information from authors about some types of materials, experimental systems and methods used in many studies. Here, indicate whether each material, system or method listed is relevant to your study. If you are not sure if a list item applies to your research, read the appropriate section before selecting a response.

Materials & experimental systems

n/a	Involved in the study
☒	☐ Antibodies
☐	☒ Eukaryotic cell lines
☒	☐ Palaeontology and archaeology
☒	☐ Animals and other organisms
☒	☐ Clinical data
☒	☐ Dual use research of concern

Methods

n/a	Involved in the study
☒	☐ ChIP-seq
☒	☐ Flow cytometry
☒	☐ MRI-based neuroimaging

Eukaryotic cell lines

Policy information about cell lines and Sex and Gender in Research

Cell line source(s)	HEK293T cells
Authentication	The cell line was thawed from previously verified cryo stocks and no further authentication was performed.
Mycoplasma contamination	The cell line was thawed from stocks previously shown to be mycoplasma free and not retested for mycoplasma contamination.
Commonly misidentified lines (See ICLAC register)	None